Supporting Material for

Late Pleistocene island weathering and precipitation in the Western Pacific Warm Pool

This PDF file includes:

Supplementary Information

Fig. S1 to S9

Supplementary Information

Regional climatic setting

A detailed overview of the different precipitation regimes found in the modern Indo-Pacific region was presented in our previous study [1]. Briefly, three climatic regions can be identified in the Indo-Pacific region based on monthly rainfall data from meteorological stations spanning 1961-1993 in the Global Historical Climatology Network (GHCN) database [2] (Fig. S1). The potential source area supplying sediments to MD01-2385 (northwestern part of New Guinea) is mostly located in region C, with higher precipitation in boreal summer, and lower precipitation in boreal winter [2] (Fig. S1). The rest of New Guinea island, however, is in region A, with the opposite rainfall seasonality: higher precipitation in austral summer, and lower precipitation in austral winter (Fig. S1). Meanwhile, region B shows biannual precipitation peaks in October–November and March–May, which are probably induced by the migration of the ITCZ [2]. In the western part (Indian Ocean), there is a relatively simple boundary between region A to the south and region B to the north. In contrast, in the eastern part (Pacific Ocean), region C displays a complex intrusion pattern, with areas to both the west and the east belonging to region A (Fig. S1). This distribution may arise from the westwards flow of the Indonesian Throughflow that transports warm water from the Pacific warm pool, thereby generating an atmospheric convection centre and bringing precipitation to the region during boreal summer, while the opposite scenario occurs during boreal winter [2]. Additionally, the monthly precipitation anomaly over the source area of MD01-2385 is highly correlated with the Southern Oscillation Index, and Niño 3.4 sea-surface temperature anomalies [1].

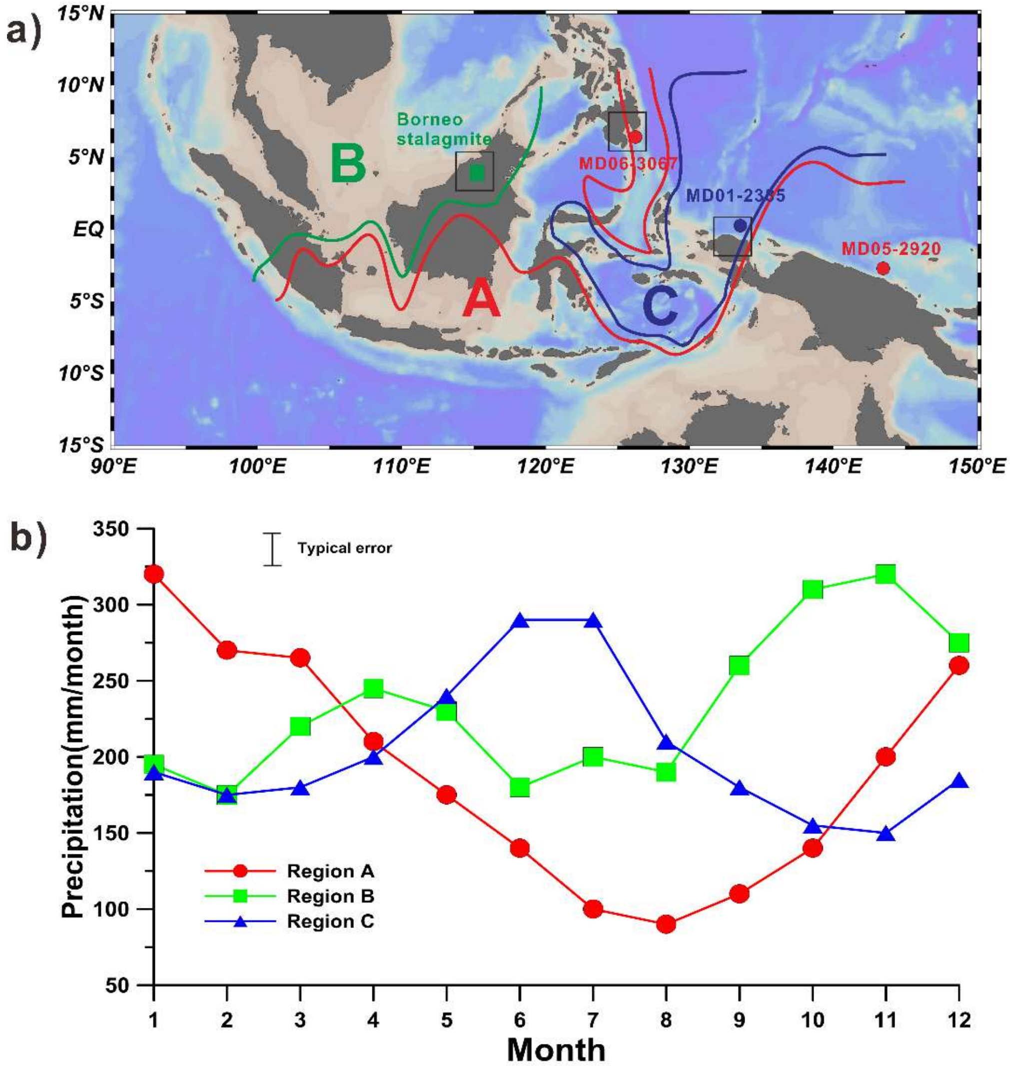

Fig. S1 Modern rainfall patterns in the Indo-Pacific region. (a) Distribution of hydrological regions A to C, based on the modern observed monthly mean rainfall patterns from the Global Historical Climatology Network (GHCN) database [2]. Locations of representative late Quaternary hydroclimate reconstructions from each region are given by dots in the same colour: MD05-2920 [3] and MD06-3067 [4] from region A (red line); Borneo stalagmite [5-7] from region B (green line); and MD01-2385 (this study) from region C (blue line). Note that region A is split into two parts by region C. The three black boxes represent the location of the simulated precipitation data used for comparison to those records (3.75° x 3.75°) [8-10]*8-10*. (b) Modern rainfall patterns in regions A (maximum in December-January), B (maximum in October-November), and C (maximum in June-July). Typical error estimate is also shown. Figure modified from Aldrian and Susanto [2].

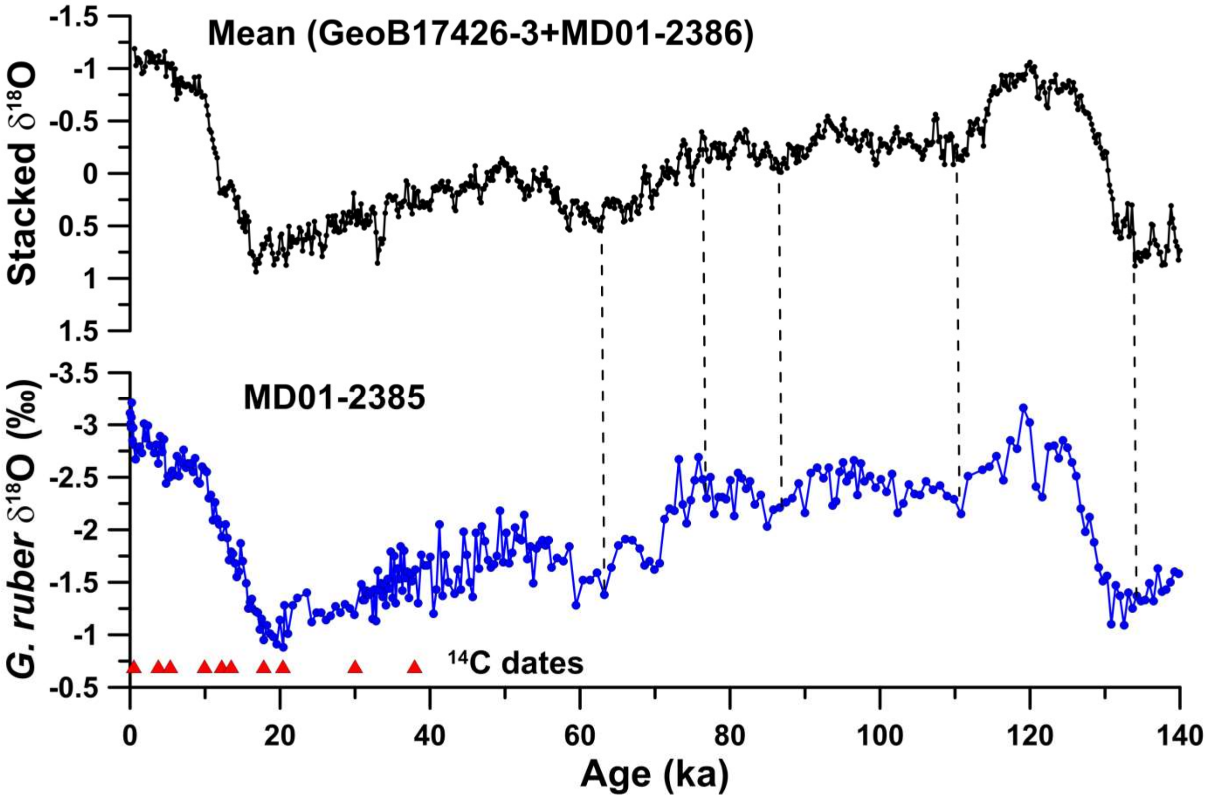

Fig. S2 Planktonic foraminiferal $\delta^{18}O$ record and age model for core MD01-2385 since 140 ka[11]. The age model from 0-40 ka is based on radiocarbon dates [1,12] (red triangles along axis). From 40-140 ka, the age model is based on tuning of the planktonic foraminifera *G. ruber* $\delta^{18}O$ record from core MD01-2385 to the stacked *G. ruber* $\delta^{18}O$ record from nearby cores GeoB17426-3 [13] and MD01-2386 [14] (tie points shown by black dashed lines; see Fig. 1b for the core locations). The age models of the latter cores were established by tuning of their benthic foraminiferal $\delta^{18}O$ records to the LR04 benthic $\delta^{18}O$ stack [15].

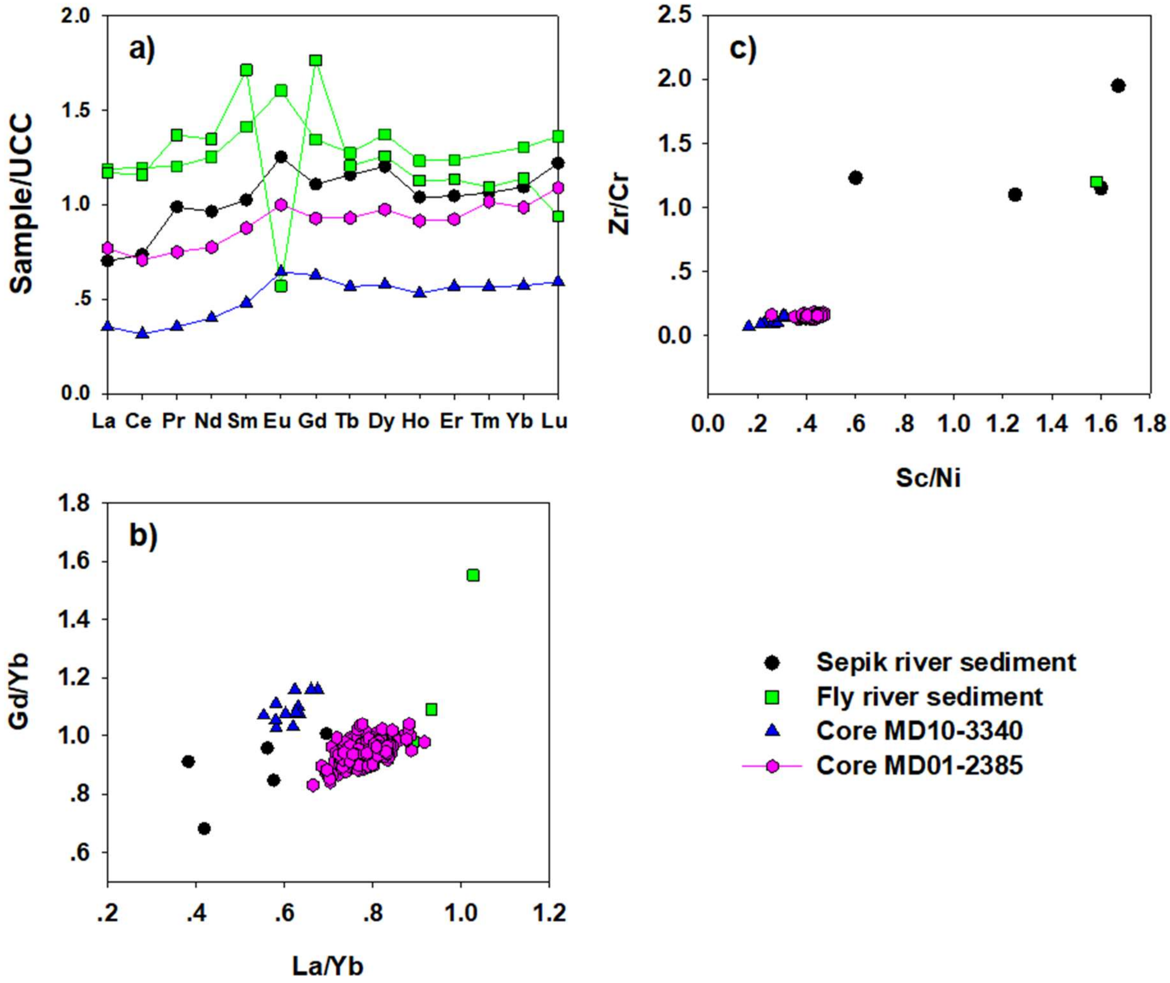

Fig. S3 (a) Average sediment REE patterns normalised to the Upper Continental Crust (UCC) [16] for Sepik river [17], Fly river [17,18], core MD10-3340 [19], and core MD01-2385 (this study). (b) UCC normalised Gd/Yb versus La/Yb in those sediments [16,20]. (c) Zr/Cr versus Sc/Ni in those sediments. These plots indicate that the sediments in core MD01-2385 are mostly supplied by local sources in northwest New Guinea via small mountainous rivers, while a significant influence from the Sepik or Fly rivers can be excluded based on their different REE patterns and/or elemental ratios.

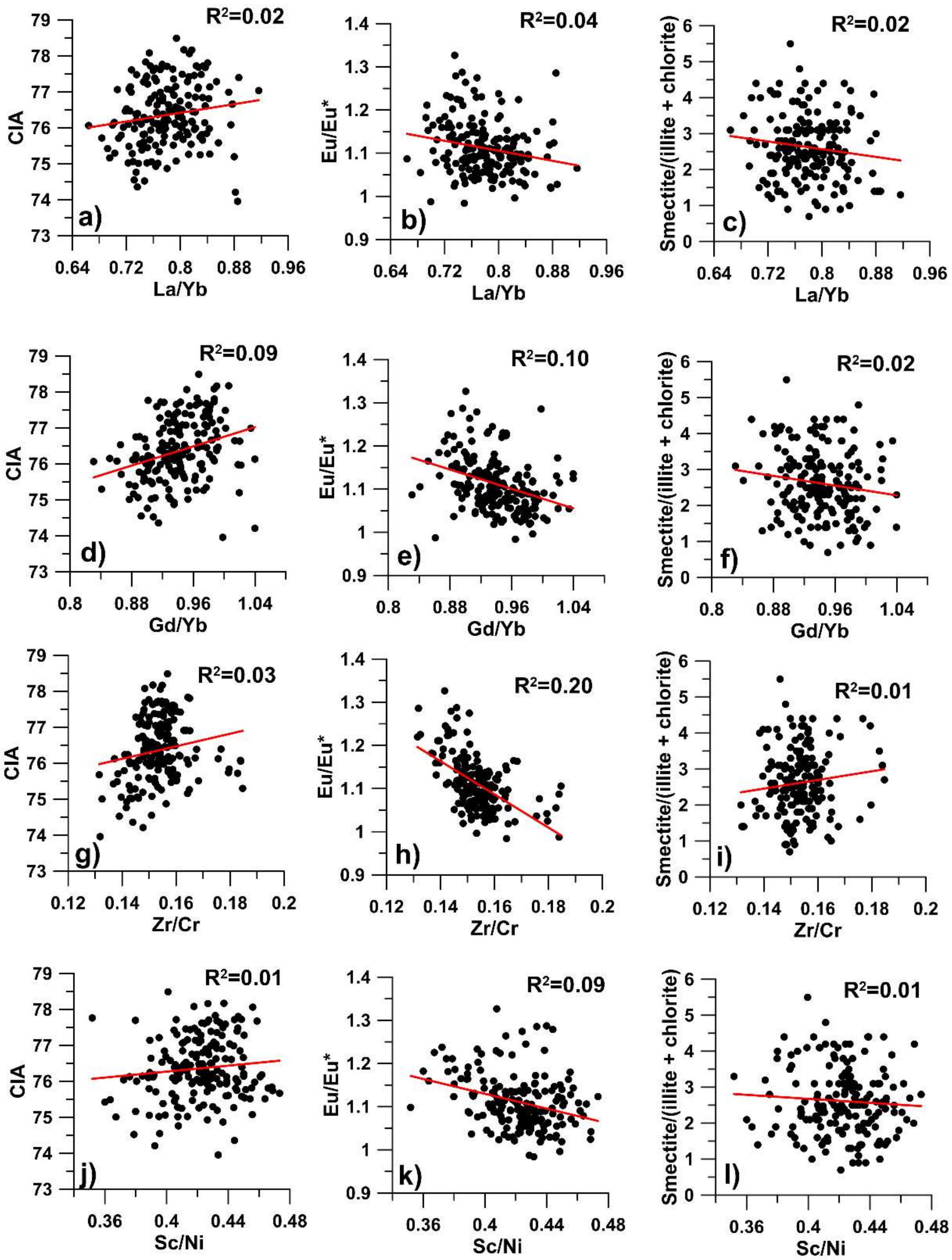

Fig. S4 Cross plots of provenance indicators (La/Yb, Gd/Yb, Zr/Cr, and Sc/Ni) with weathering and erosion proxies (CIA, Eu/Eu*, and smectite/(illite+chlorite) ratios) in core MD01-2385. La/Yb and Gd/Yb are UCC-normalised data [16,20]. The lack of obvious correlations implies that there is an insignificant effect of sediment source changes on the weathering and erosion proxies.

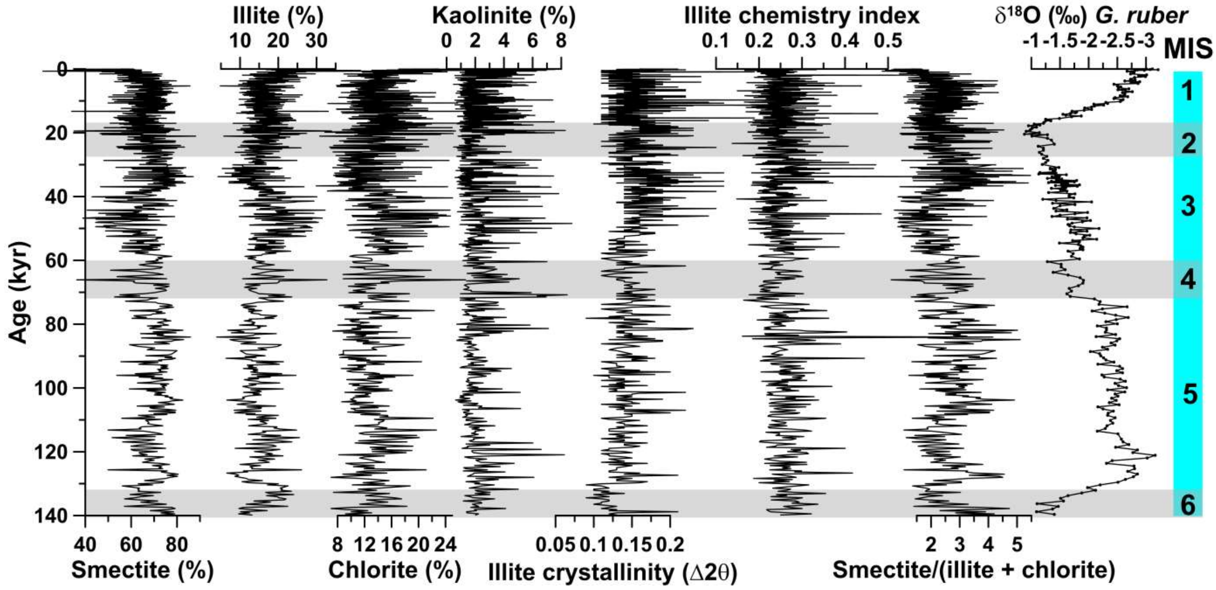

Fig. S5 Downcore records of clay mineralogy in core MD01-2385. Also shown are the planktonic foraminifera G. *ruber* $\delta^{18}O$ record from core MD01-2385 (this study) and the timing of marine isotope stages (MIS) 1 to 6. Grey shaded bars indicate glacial periods (MIS 2, 4, and 6).

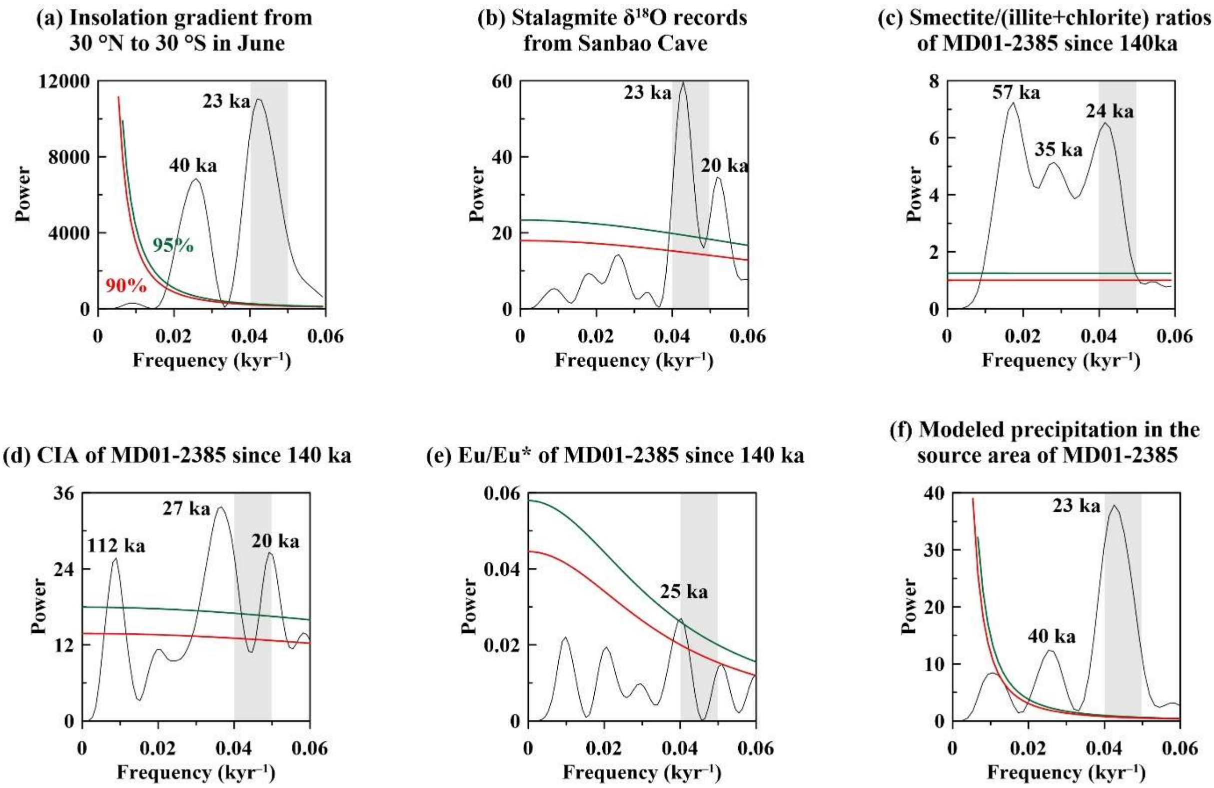

Fig. S6 Spectral analysis of (a) insolation gradient from 30 °N to 30 °S in June [21], (b) stalagmite $\delta^{18}O$ records from Sanbao Cave [22], (c) smectite/(illite+chlorite) ratios in core MD01-2385 since 140 ka (this study), (d) CIA in core MD01-2385 since 140 ka (this study), (e) Eu/Eu* in core MD01-2385 since 140 ka (this study), and (f) modelled precipitation in the source area of MD01-2385 [8-10]. The spectral analysis was performed with PAST software; the window function is rectangle; the oversample is 8; the segment is 2 for (a), (c), and (f), and is 1 for (b), (d), and (e). The 95% and 90% confidence curves are represented by green and red lines, respectively. The grey bars indicate a periodicity of 20-25 kyr.

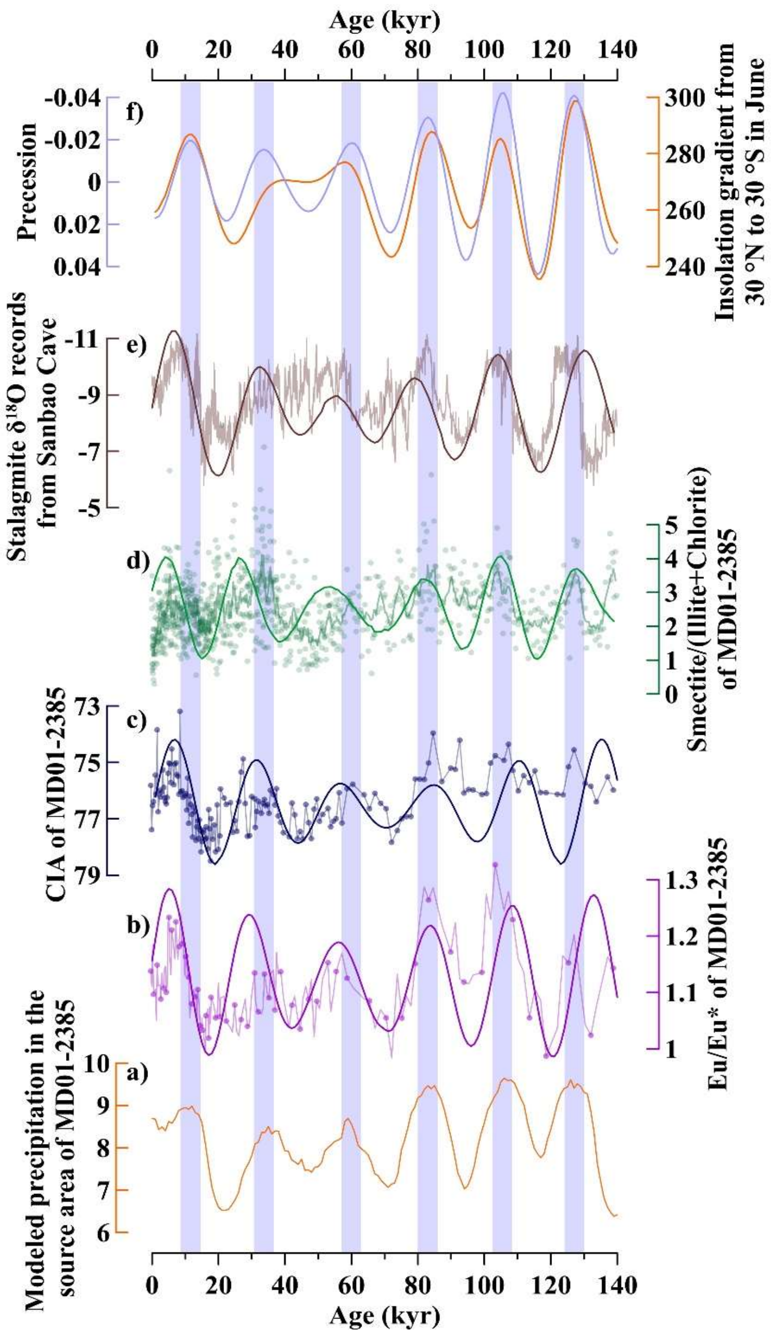

Fig. S7 Similar precession-dominated cycles in (a) modelled precipitation in the source area of core MD01-2385, (b) Eu/Eu* in core MD01-2385, (c) CIA in core MD01-2385, (d) smectite/(illite+chlorite) in core, (e) stalagmite $\delta^{18}O$ records from Sanbao Cave [22], and (f) north-south insolation gradient (orange) and precession (purple) [21]. The pale points and lines in (b-e) represent the raw data. The superimposed curves are precessional band-pass filtered data (b-e), filtered by PAST with a central frequency of 0.043 kyr^{-1} and a bandwidth of 0.01 kyr^{-1}. The light purple shaded bars represent the precession minima.

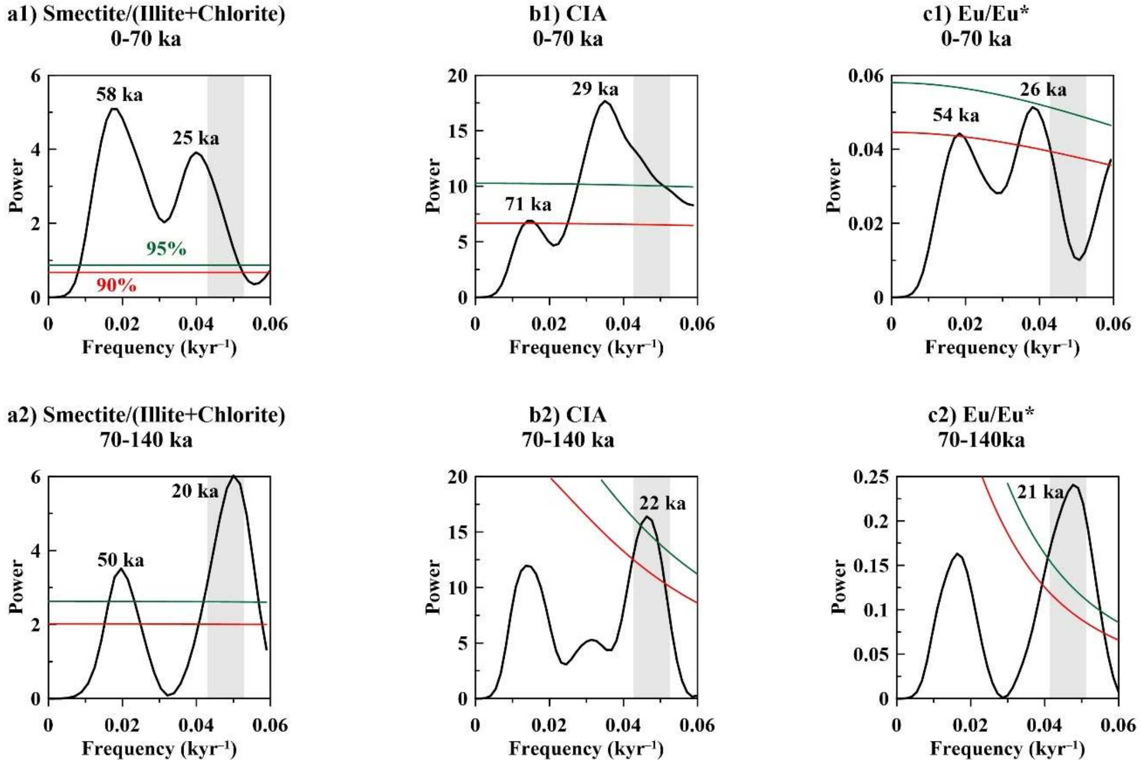

Fig. S8 Spectral analysis of weathering records: (a) smectite/(illite+chlorite); (b) CIA; (c) Eu/Eu* in core MD01-2385 between the period 0-70 ka (upper, labelled 1) and 70-140 ka (lower, labelled 2). The spectral analysis was performed with PAST software with a rectangle window function; the oversample is 10; the segment is 1. The 95% and 90% confidence curves are represented by green and red lines, respectively. The grey bars indicate a periodicity of 19-23 kyr.

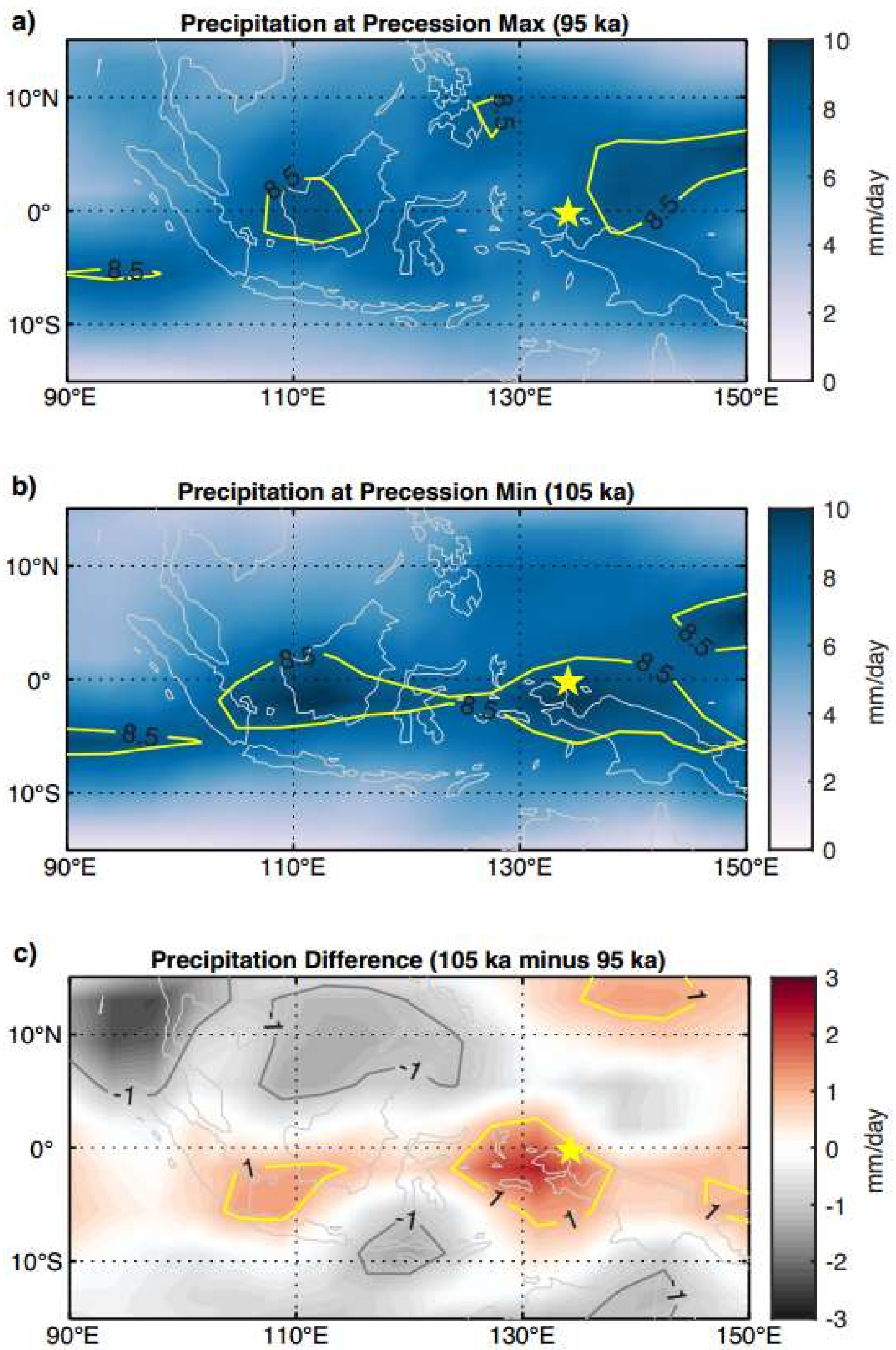

Fig. S9 Precipitation over the Indo-Pacific region simulated by CESM during (a) precession maximum (95 ka), (b) precession minimum (105 ka), and (c) their difference (105 ka minus 95 ka) 8-10. See also Fig. 5 in the main text.

References

1 Yu, Z. *et al.* Millennial-scale precipitation variability in the Indo-Pacific region over the last 40 kyr. *Geophysical Research Letters* **n/a**, e2022GL101646 (2023). https://doi.org/https://doi.org/10.1029/2022GL101646

2 Aldrian, E. & Susanto, R. Identification of three dominant rainfall regions within Indonesia and their relationship to sea surface temperature. *International Journal of Climatology: A Journal of the Royal Meteorological Society* **23**, 1435-1452 (2003).

3 Tachikawa, K. *et al.* The precession phase of hydrological variability in the Western Pacific Warm Pool during the past 400 ka. *Quaternary Science Reviews* **30**, 3716-3727 (2011). https://doi.org/https://doi.org/10.1016/j.quascirev.2011.09.016

4 Kissel, C. *et al.* Monsoon variability and deep oceanic circulation in the western equatorial Pacific over the last climatic cycle: Insights from sedimentary magnetic properties and sortable silt. *Paleoceanography* **25** (2010).

5 Carolin, S. A. *et al.* Northern Borneo stalagmite records reveal West Pacific hydroclimate across MIS 5 and 6. *Earth and Planetary Science Letters* **439**, 182-193 (2016). https://doi.org/https://doi.org/10.1016/j.epsl.2016.01.028

6 Carolin, S. A. *et al.* Varied response of western Pacific hydrology to climate forcings over the last glacial period. *Science* **340**, 1564-1566 (2013).

7 Partin, J. W., Cobb, K. M., Adkins, J. F., Clark, B. & Fernandez, D. P. Millennial-scale trends in west Pacific warm pool hydrology since the Last Glacial Maximum. *Nature* **449**, 452-455 (2007).

8 Ruan, J. *et al.* Climate shifts orchestrated hominin interbreeding events across Eurasia. *Science* **381**, 699-704 (2023). https://doi.org/10.1126/science.add4459

9 Timmermann, A. *et al.* Climate effects on archaic human habitats and species successions. *Nature* **604**, 495-501 (2022). https://doi.org/10.1038/s41586-022-04600-9

10 Yun, K.-S. *et al.* A transient coupled general circulation model (CGCM) simulation of the past 3 million years. *Clim. Past* **19**, 1951-1974 (2023). https://doi.org/10.5194/cp-19-1951-2023

11 Tang, X. *et al.* Orbital hydroclimate variability revealed by grain-size evidence in the tropical Pacific Islands since 140 ka. *Global and Planetary Change*, 104429 (2024). https://doi.org/https://doi.org/10.1016/j.gloplacha.2024.104429

12 Wu, Q. *et al.* Foraminiferal εNd in the deep north-western subtropical Pacific Ocean: Tracing changes in weathering input over the last 30,000years. *Chemical Geology* **470**, 55-66 (2017). https://doi.org/https://doi.org/10.1016/j.chemgeo.2017.08.022

13 Hollstein, M. *et al.* The impact of astronomical forcing on surface and thermocline variability within the Western Pacific Warm Pool over the past 160 kyr. *Paleoceanography and Paleoclimatology* **35**, e2019PA003832 (2020).

14 Jian, Z. *et al.* Half-precessional cycle of thermocline temperature in the western equatorial Pacific and its bihemispheric dynamics. *Proceedings of the National Academy of Sciences* **117**, 7044-7051 (2020).

15 Lisiecki, L. & Raymo, M. A Pliocene-Pleistocene stack of 57 globally distributed benthic $\delta^{18}O$ records. *Paleoceanography* **20, PA1003** (2005).

16 Rudnick, R., Gao, S., Holland, H. & Turekian, K. Composition of the continental crust. *The crust* **3**, 1-64 (2003).

17 Hannigan, R. E. & Sholkovitz, E. R. The development of middle rare earth element enrichments in freshwaters: weathering of phosphate minerals. *Chemical Geology* **175**, 495-508 (2001). https://doi.org/https://doi.org/10.1016/S0009-2541(00)00355-7

18 Bayon, G. *et al.* Rare earth elements and neodymium isotopes in world river sediments revisited. *Geochimica et Cosmochimica Acta* **170**, 17-38 (2015).

19 Dang, H., Jian, Z., Kissel, C. & Bassinot, F. Precessional changes in the western equatorial Pacific Hydroclimate: A 240 kyr marine record from the Halmahera Sea, East Indonesia. *Geochemistry, Geophysics, Geosystems* **16**, 148-164 (2015).

20 Evensen, N. M., Hamilton, P. & O'nions, R. Rare-earth abundances in chondritic meteorites. *Geochimica et cosmochimica Acta* **42**, 1199-1212 (1978).

21 Laskar, J. *et al.* A long-term numerical solution for the insolation quantities of the Earth. *Astronomy & Astrophysics* **428**, 261-285 (2004).

22 Cheng, H. *et al.* The Asian monsoon over the past 640,000 years and ice age terminations. *Nature* **534**, 640-646 (2016).